Available online at www.sciencedirect.com
ScienceDirect
Trans. Nonferrous Met. Soc. China 28(2018) 1640−1651
Transactions of Nonferrous Metals Society of China
www.tnmsc.cn

Mineralogy, liberation and leaching characteristics of iron oxide phases in an Indian diaspore sample

Danda Srinivas RAO, Swagat S. RATH, Nilima DASH, Swagatika MOHANTY, Surendra K. BISWAL

Council of Scientific and Industrial Research, Institute of Minerals and Materials Technology, Bhubaneswar 751013, India

Received 18 August 2017; accepted 4 April 2018

Abstract: The removal of iron from an Indian diaspore sample was studied using magnetic separation and leaching techniques aided by an in-depth mineralogical characterization study involving quantitative mineralogical evaluation by scanning electron microscope (QEMSCAN), electron probe micro-analyzer (EPMA) and X-ray diffraction (XRD). The characterization studies indicate that extremely fine-sized hematite grains are associated with several other mineral phases in a complex manner with around 60% of the hematite not liberated even below the size of 38 μm limiting the scope of physical separation processes to remove the iron. Wet high intensity magnetic separation (WHIMS) studies reveal that only 49% of iron can be removed. Further, leaching studies using oxalic acid suggest that around 76% of the iron can be removed under conditions such as a solid to liquid ratio of 0.05:1, a temperature of 90 °C, a time period of 120 min and an acid concentration of 1 mol/L. The dissolution of iron in oxalic acid is found to be controlled by chemical reaction and the activation energy is calculated as 35.15 kJ/mol.
Key words: diaspore; liberation; mineralogy; leaching; magnetic separation

1 Introduction

Bauxite is an important aluminium reserve consisting of minerals such as gibbsite, boehmite, and diaspore, in association with other minerals such as kaolinite, quartz, hematite, and anatase [1]. While the extraction of alumina continues to be the major application of bauxite, several other industries dealing with abrasives, refractory and pottery use it as a raw material. Gibbsite is mostly exploited as the principal source of aluminium while diaspore finds its major application in making high-alumina refractory bricks either by itself or by bonding with flint or plastic clay as per the content of alumina needed in the finished product. Apart from that, it is used as filler in plastic industry [2]. So far as the Indian context is concerned, out of the total resources of diaspore, around 76% is of refractory grade and less than 1% is ceramic grade and the rest belongs to unclassified categories [2]. The Bayer's process, which is the most adopted means of industrial refining of bauxite for extracting alumina, favours a low content of iron in order to have a lesser generation of red mud. Moreover, the other applications of diasporic bauxite as discussed above demand very low iron content. For example, the iron oxide content should be less than 2% for refractory purposes [3] and below 0.1% for ceramic applications [4]. Therefore, the removal of iron oxide from diaspore is an important problem to tackle. The separation of iron and silica has been the focus of many research articles related to diaspore. There have been several attempts to remove iron from bauxite, which include magnetic separation [5], pyro-chemical treatment [6,7] and leaching using both biological [8] and acidic routes [3,9]. However, similar work relevant to the removal of iron from diasporic bauxite is scanty. PASPALIARIS and TSOLAKIS [10] carried out the leaching of a diaspore sample from Greece using hydrochloric acid, studied its kinetics and found that the residue still contains iron to the tune of 5% even after leaching under optimum conditions. They attributed it to the isomorphous replacement of Al atoms by iron atoms in the diaspore crystal lattice. Similarly, the dissolution kinetics of HCl leaching of a diasporic bauxite sample from Turkey was studied, where 96.46% of the iron could be leached out [11]. Recently, LI et al [12] carried out the extraction of aluminum, iron, and titanium bearing constituents from diaspore-type bauxite ores by stepwise treatment consisting of

Corresponding author: Swagat S. RATH; Tel: +91-674-2379147; Fax: +91-674-2581160; E-mail: ssrath@immt.res.in
DOI: 10.1016/S1003-6326(18)64807-1

predesilication via alkali-leaching of diaspore, extraction of alumina via Bayer's process, and recovery of iron from red mud via magnetic separation. It may be noted that the separation of Al and Fe in complex ores is an important research topic and various attempts such as direct reduction of lateritic ore [13], soda-ash roasting of high Al-containing hematite [14] and reductive roasting of red mud [15] have been reported. Other than these, many Chinese workers have concentrated on enhancing the alumina to silica ratio through flotation techniques as diaspore is the main alumina resource of China [16]. Therefore, much attention has been given towards developing different flotation collectors [17,18] and depressants [19,20] for diaspore.

The study of liberation of mineral constituents of any complex ore body is important in order to select a feasible beneficiation methodology. Though there have been a few attempts relevant to the characterization of diaspore [21], the literature pertaining to the characterization with a special reference to the association and liberation of iron minerals is limited. Most of the work relevant to the physical beneficiation of bauxite does not provide any information on the liberation pattern. Considering the above discussion, the present work is intended towards understanding the geochemistry and liberation of a diaspore sample collected from Bundelkhand complex, Uttar Pradesh, India. Further attempts have been taken to remove the iron impurity using both magnetic separation and leaching using an organic acid such as oxalic acid instead of strong inorganic acids like HCl. Along with that kinetics studies have been undertaken to understand the rate controlling mechanism of iron dissolution from diaspore in the oxalic acid medium.

2 Experimental

2.1 Sample

The diaspore sample used in this study was obtained from a working mine of Uttar Pradesh, India. The handpicked samples, when subjected to wet chemical analysis exhibited a wide range of compositions, which are listed in Table 1. The quantity of Al_2O_3 in different samples varied between 37.49% and 68.62% while Fe_2O_3 and SiO_2 ranged from 1.21% to 12.99% and 13.28% to 39.38% respectively. However, a representative bulk sample was prepared for the present work, from the run of mines (ROM) sample, by standard coning and quartering method and the chemical composition of the same was found to be 58.3% Al_2O_3, 18.1% SiO_2, 7.9% Fe and loss on ignition (LOI) of 12.3%. The XRD spectra of the sample as shown in Fig. 1 indicate the presence of diaspore, kaolinite, fluorapatite and hematite as the major phases.

Table 1 Chemical compositions of some handpicked diaspore samples

Sample No.	$w(Al_2O_3)$/%	$w(Fe_2O_3)$/%	$w(SiO_2)$/%
1	68.62	1.21	13.28
2	54.22	9.43	28.50
3	37.49	12.99	39.38
4	42.81	8.91	35.71
5	52.61	6.96	30.31
6	60.21	5.86	23.92
7	58.25	7.24	24.87
8	52.42	6.39	30.78
9	54.21	7.08	28.51
10	55.01	8.38	26.18

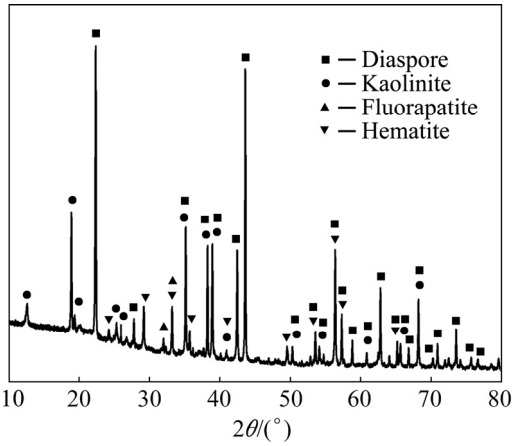

Fig. 1 XRD pattern of diaspore bulk sample

2.2 Characterization

The characterization studies were carried out by XRD, SEM−EDS, QEMSCAN and EPMA. The polished sections for all the characterization studies were prepared as per standard conventional techniques using grinding and polishing. The XRD studies were carried out by Philips X-ray diffractometer using Cu K_α radiation (PANalytical, X'pert) operated at 40 kV and 30 mA in order to investigate the different mineral phases present in the sample. The polished sections were studied under the SEM (Zeiss make) and EPMA (Jeol JXA 8200 model) for understanding the quantitative mineralogy and semi-quantitative elemental chemistry while the liberation characteristics of iron minerals were studied using QEMSCAN (M/s. Intellection Pty. Ltd., Australia) instrument. It may be noted that QEMSCAN is a fully automated micro-analysis system that determines not only the quantitative percentage of mineral phases but also generates quantitative liberation characteristics of the different constituents in the ore. The working details of the QEMSCAN have been described elsewhere [22,23].

2.3 Magnetic separation

Magnetic separation studies were conducted by a laboratory model of Wet High-Intensity Magnetic Separator (WHIMS) supplied by Box Mag Rapid, England. The magnetic intensities of 7700−15400 Gauss were applied during the course of the experiments. Several experiments were carried out by varying the magnetic intensity and particle size.

2.4 Leaching

Leaching studies were carried out using oxalic acid ($C_2H_2O_4$, reagent grade). The experiments were performed in a 250 mL glass vessel placed on a magnetic stirrer having temperature control. All the leaching tests were conducted at atmospheric pressure. The diaspore sample ground to below 38 μm was treated with 100 mL of the oxalic acid-water solution of a desired concentration while maintaining the required solid to liquid ratio and temperature. The agitation rate was fixed at 700 r/min. On completion of the experiment, the filtered leach liquor was subjected to iron analysis using atomic absorption spectrometry (AAS).

3 Results and discussion

3.1 Mineralogy and mineral chemistry

A representative diaspore sample was ground and sieved to six different size fractions such as 500−1000 μm, 250−500 μm, 125−250 μm, 75−150 μm, 38−75 μm, and <38 μm. The polished section of each size fraction was studied under QEMSCAN for quantitative mineralogy and liberation analysis. The quantification of different mineral phases in the sample was determined using the QEMSCAN system and the compositions of the phases in all the size fractions are listed in Table 2. The results indicate that, quantity wise, the diaspore mineral constitutes 68.92% by mass of the sample, which is distantly followed by hematite accounting for 9.26% by mass. The size fractions of 500−1000 μm and 250−500 μm contain majority of the diaspore and hematite phases. The presence of muscovite, chlorite, apatite and kaolinite ranging from ~2% to 4% is also observable from the data presented in Table 2.

The mineralogical studies, with the help of SEM−EDS also supported the above finding that the sample contains diaspore as the major mineral with hematite, muscovite, chlorite, apatite and kaolinite as the major gangue minerals along with traces of quartz, barite, ilmenite, rutile, phlogopite, biotite, zircon, tourmaline, almandine and calcite. Out of all these minerals, hematite is the major iron bearing mineral contributing to the iron content of the ore, thereby degrading the quality of the diaspore sample for industrial applications. In addition, traces of ilmenite and orthochamosite also contribute towards the iron content in the sample. Other important associated minerals include apatite (fluorapatite) and gorceixite as the phosphorus bearing minerals, and zircon as the zirconium bearing mineral.

Table 2 Quantitative mineralogy of diaspore sample

Mineral	*w*/%						Total/%
	500−1000 μm	250−500 μm	150−250 μm	75−150 μm	38−75 μm	<38 μm	
Diaspore	32.84	16.57	3.88	4.96	3.71	6.96	68.92
Hematite	3.18	2.58	0.56	0.91	0.56	1.47	9.26
Muscovite	1.49	1.02	0.2	0.27	0.25	0.8	4.03
Chlorite	1.12	0.96	0.26	0.32	0.28	1.07	4.01
Apatite	1.3	0.42	0.14	0.24	0.27	0.4	2.77
Kaolinite	1	0.63	0.16	0.19	0.15	0.62	2.75
Barite	0.31	0.19	0.04	0.05	0.03	0.07	0.69
Quartz	0.08	0.04	0.01	0.02	0.02	0.09	0.26
Ilmenite	0.09	0.09	0.02	0.03	0.02	0.04	0.29
Rutile	0.13	0.05	0.01	0.02	0.01	0.03	0.25
Phologopite	0.06	0.03	0.01	0.01	0.01	0.01	0.13
Biotite	0.01	0.03	0.01	0.01	0.01	0.01	0.08
Zircon	0.02	0.01	0	0.01	0.02	0.01	0.07
Tourmaline	0.01	0.01	0	0	0	0	0.02
Almandine	0.07	0.05	0.02	0.02	0.02	0.04	0.22
Calcite	0	0	0	0	0.01	0.07	0.08
Orthochamosite	0	0	0.05	0.07	0.02	0.07	0.21

The back scattered image (BSE) as shown in Fig. 2 displays numerous shapes and sizes of apatite occurring in association with anhedral hematite as well as with various silicate phases. The numbers on these photomicrographs indicate that the points were analyzed by SEM−EDS and reported in Table 3.

Notably, diaspore is found to occur in the shape of elongated needles within silicates (Fig. 3), whereas zircon and apatite are associated with granular diaspore (Fig. 3). Lath as well as needle-shaped hematite grains are also observed (Fig. 4) and gorceixite is found enclosed within diaspore (Fig. 4). Various shapes and sizes of apatite and hematite as inclusions are observed in the EPMA elemental mapping as shown in Fig. 5. Similarly, apatite and zircon can be located as inclusions within diaspore, which is evident from Fig. 6.

The semi-quantitative mineral chemistry of various phases of the diaspore sample is presented in Table 3.

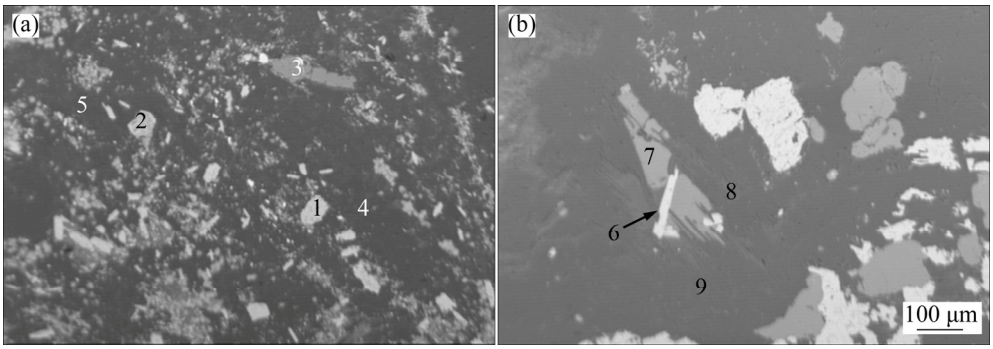

Fig. 2 BSE images showing association of hematite and apatite in diaspore sample: (a) Various shapes and sizes of hematite (1 and 2) and lath shaped apatite (3) within diaspore (4 and 5); (b) Numerous shapes and sizes of apatite (7) as well as anhedral hematite (6) grains within diaspore (8 and 9)

Table 3 SEM−EDS semi-quantitative mineral chemistry of various mineral phases of diaspore sample

Number shown in Figs. 2−4	*w*/%														
	O	Mg	Al	Si	Ti	Fe	Co	Ba	F	P	Ca	K	Na	Zr	Hf
1	23.8	0.04	0.17	0.06	2.24	71.3	1.48	0.9	−	−	−	−	−	−	−
2	23.4	0.07	1.04	0.54	1.96	70.3	1.51	1.17	−	−	−	−	−	−	−
3	33.7	0.11	−	−	−	0.21	−	−	4.74	17.8	43.5	−	−	−	−
4	54.2	0.23	42.1	1.13	0.24	1.38	0.07	−	−	−	−	0.64	−	−	−
5	53.1	0.22	46	−	0.13	0.59	−	−	−	−	−	−	−	−	−
6	27.2	0.07	0.83	−	1.15	68.8	1.28	0.56	−	−	0.1	−	−	−	−
7	27.4	−	0.18	−	−	−	−	−	12.1	17.8	42.1	−	0.39	−	−
8	52.8	0.22	45.6	0.77	0.13	0.51	−	−	−	−	−	−	−	−	−
9	53	−	18.7	27.5	−	0.77	−	−	−	−	−	−	−	−	−
10	45.9	5.87	16.9	9.44	−	21.7	−	−	−	−	0.03	0.15	−	−	−
11	52.5	0.28	46.5	−	0.13	0.5	−	0.09	−	−	−	−	−	−	−
12	47.5	5.47	15.9	8.54	−	22.5	−	−	−	−	−	0.11	−	−	−
13	52.8	0.27	46.2	−	0.33	0.4	−	−	−	−	−	−	−	−	−
14	22.9	−	0.06	13.6	−	0.43	−	−	−	−	0.08	−	−	60.7	2.29
15	28.1	−	−	0.04	−	−	−	−	11.9	17.5	42.1	−	0.25	−	−
16	55	0.18	44.4	−	0.1	0.31	−	−	−	−	0.02	−	−	−	−
17	68.7	−	10.6	0.53	−	1.61	−	10.9	−	7.26	0.45	−	−	−	−
18	59.5	−	13.5	0.83	−	2.91	−	13.3	−	9.16	0.46	−	0.36	−	−
19	53	0.21	45.9	−	0.23	0.56	−	0.1	−	−	−	−	−	−	−
20	53	0.24	45.9	0.21	0.12	0.43	−	0.12	−	−	−	−	−	−	−

Numbers 1, 2, 6 are hematite; numbers 3, 7, 15 are apatite; number 14 is zircon; numbers 4, 5, 8, 11, 13, 16, 19 and 20 are diaspore; number 9 is kaolinite; numbers 17 and 18 are gorceixite; numbers 10 and 12 are orthochamosite

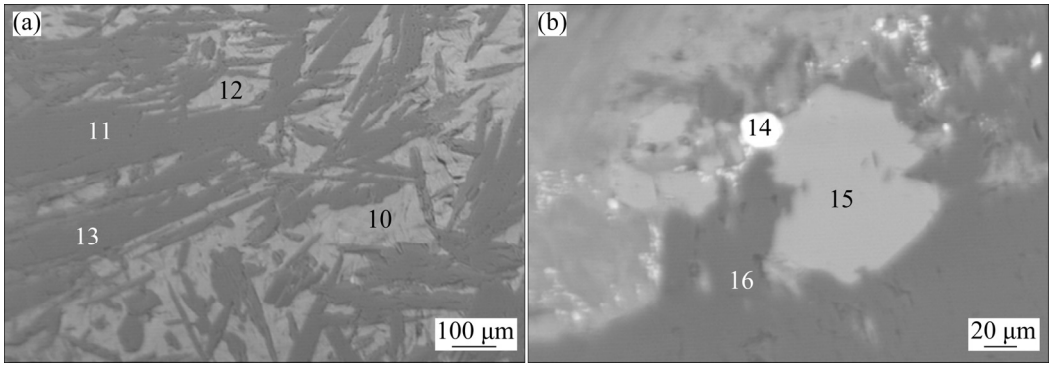

Fig. 3 BSE images showing the presence of orthochamosite and zircon in sample: (a) Elongated needle-shaped diaspore (11 and 13) within orthochamosite (10 and 12); (b) Zircon (14) and apatite (15) within diaspore

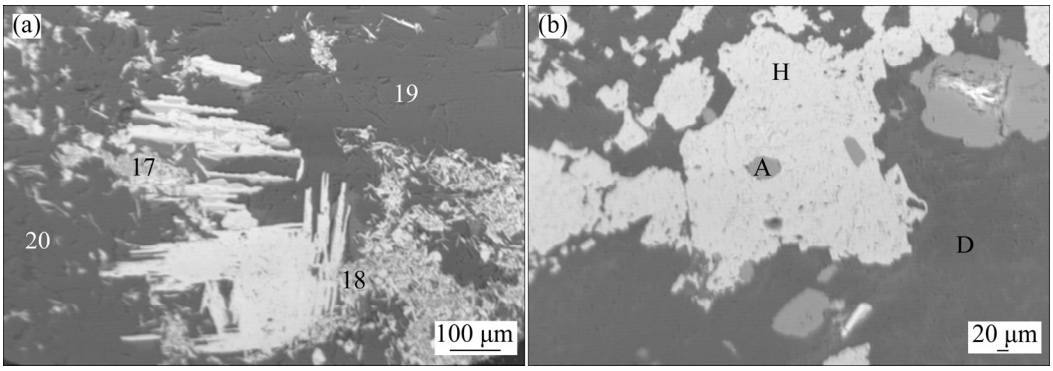

Fig. 4 BSE images showing association of hematite, gorceixite and apatite in sample: (a) Lath and needle-shaped hematite (white) and gorceixite (17 and 18) enclosed within diaspore (19 and 20); (b) Apatite (A) with hematite (H) and hematite within diaspore (D)

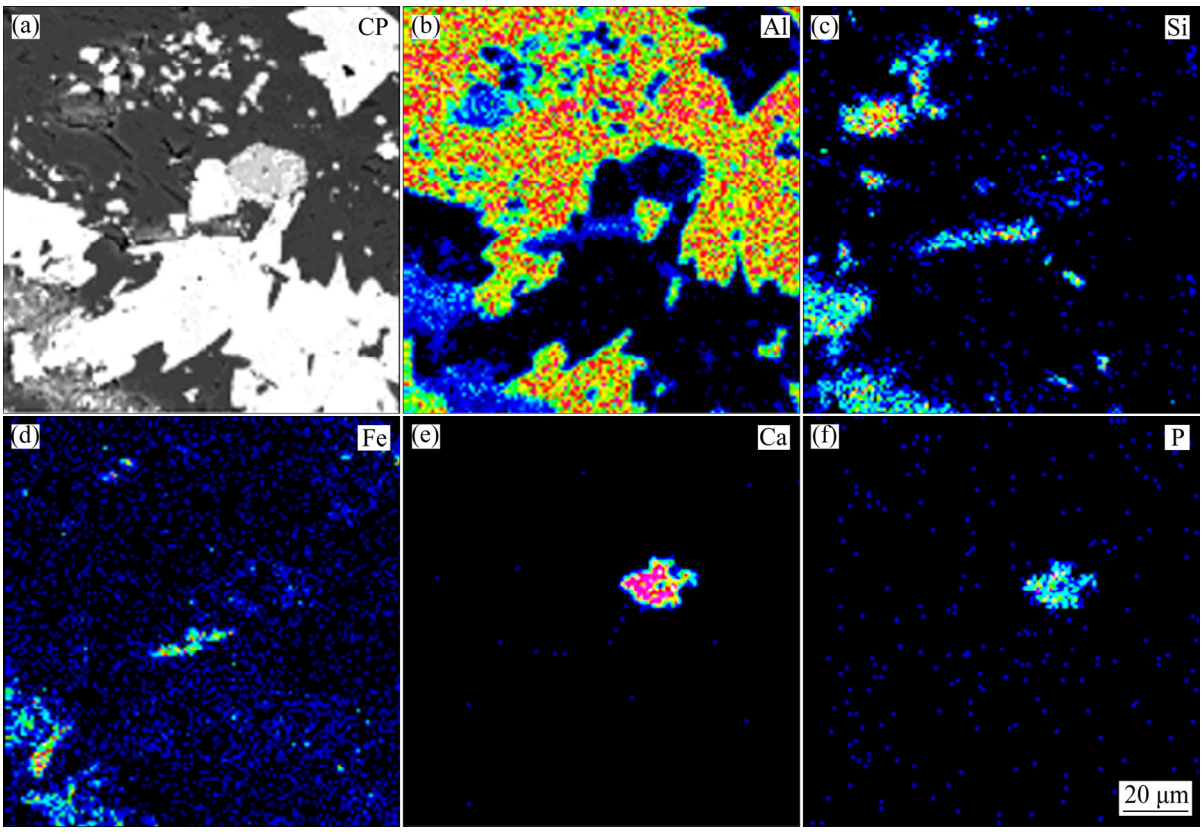

Fig. 5 Elemental mapping of diaspore sample showing the presence of apatite and hematite (CP—Compositional image)

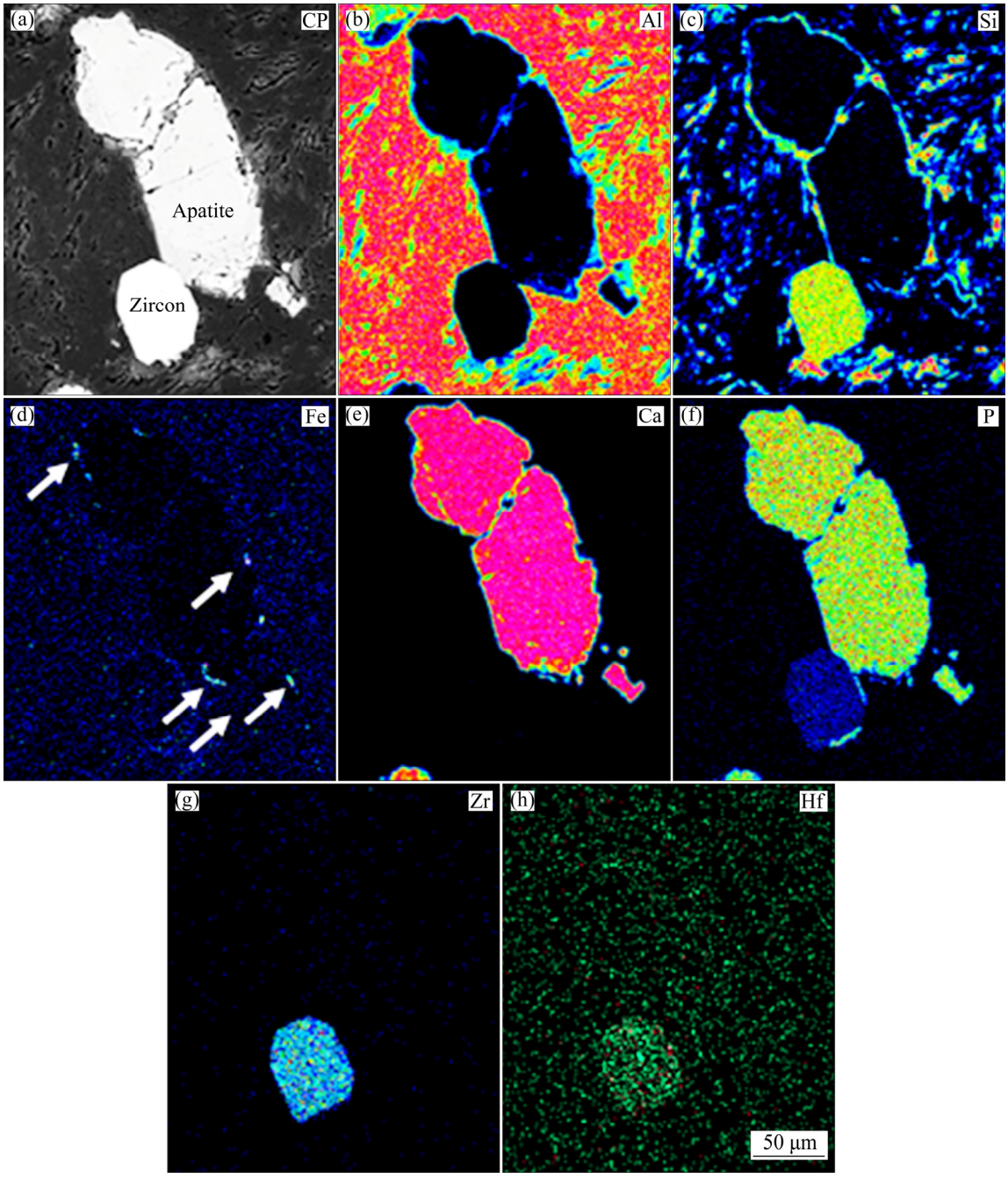

Fig. 6 Elemental mapping of diaspore sample showing the presence of apatite and zircon

Significant amount of Ti (1.15%−2.24%), Ba (0.56% to 1.17%) and Co (1.28% to 1.51%) were recorded in the hematite phases. However, gorceixite is the significant barium-bearing mineral phase in this diaspore sample, wherein the barium oxide content ranges from 10.85% to 13.30%. Gorceixite is also a phosphorous-bearing mineral with 7.26%−9.16% P_2O_5. Apatite is a fluorine-bearing phase (4.74%−12.11%) and hence, can be termed as fluorapatite. Zircon, which occurs as inclusion contains significant amounts of Hf (2.29%). Orthochamosite is a rare hydroxyl-bearing iron magnesium aluminum silicate mineral also present in the sample contributing iron to the sample.

3.2 Liberation characteristics

The liberation patterns of hematite in the five size fractions such as 500−1000, 250−500, 125−250, 75−150, 38−75, and <38 μm were studied using QEMSCAN. The quantitative data of degree of liberation in various size fractions are presented in Table 4. The data suggest that 7.26% of the hematite particles by mass are fully liberated while only 3.99% of hematite particles have a degree of liberation from 90% to 100%. Around 67.48% by mass of the hematite particles have liberation less than 50%. Moreover, it is observed that the majority of the particles having more than 90% liberation report in the fine size fractions, i.e., below 75 μm. Even below

Table 4 Mass fraction of hematite liberation with respect to size

Degree of hematite liberation/%	Mass fraction of hematite/%						Total/%
	500−1000 μm	250−500 μm	150−250 μm	75−150 μm	38−75 μm	<38 μm	
0−10	25.70	13.50	11.69	8.35	7.31	3.53	15.13
10−20	22.39	15.75	14.98	9.56	8.55	7.97	15.71
20−30	28.05	11.97	11.08	6.74	6.55	5.72	15.62
30−40	13.16	13.32	9.21	7.00	4.93	9.42	11.27
40−50	6.40	15.18	8.97	7.06	5.36	11.09	9.75
50− 60	4.30	7.63	5.74	8.31	5.98	3.74	5.72
60−70	0.00	7.31	9.21	6.39	6.60	5.51	4.49
70−80	0.00	8.32	9.41	7.86	9.01	6.39	5.21
80−90	0.00	6.19	11.07	14.70	16.77	6.32	5.85
90−100	0.00	0.40	7.24	18.98	9.90	6.22	3.99
100	0.00	0.43	1.41	5.05	19.05	34.07	7.26

38 μm, only 34.07% by mass of hematite particles are 100% liberated. Again, the majority of the hematite particles present in the coarser fractions such as 500−1000 μm, 250−500 μm, 125−250 μm have a degree of liberation below 30%−40%. For example, the fraction 500−10000 μm contains 89.3% by mass of hematite particles which have liberation below 40%. These results suggest that hematite has a poor liberation in the sample.

Further, mineral mapping of two size fractions namely, 500−1000 μm and 250−500 μm as shown in Figs. 7 and 8 indicates the locking and liberation characteristics of the minerals in the sample. The mapping gives a clear picture of the complex liberation pattern of the minerals.

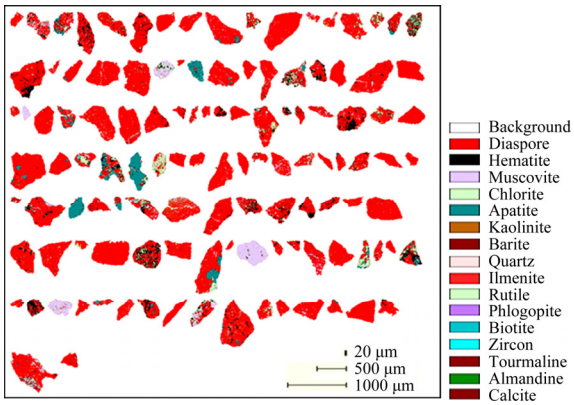

Fig. 7 Mineral mapping of sample with 500−1000 μm size fraction

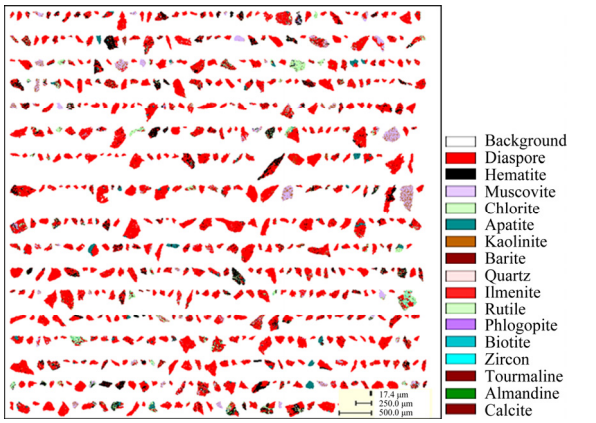

Fig. 8 Mineral mapping of sample with 250−500 μm size fraction

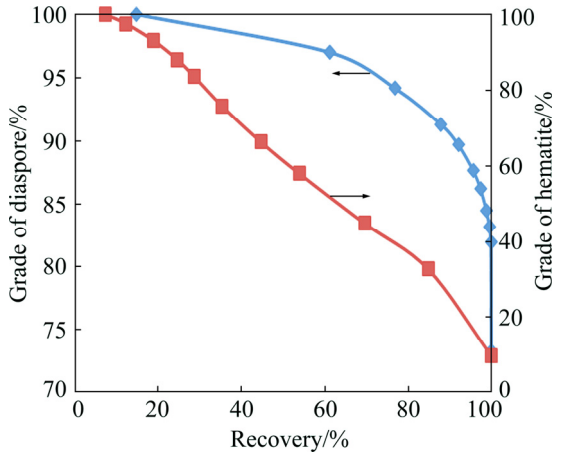

Fig. 9 Theoretical grade recovery curves of diaspore and hematite from QEMSCAN data

The QEMSCAN data were further utilized to generate the theoretical grade−recovery graph as shown in Fig. 9. The theoretical grade−recovery curve of an ore refers to the maximum expected recovery by flotation of any mineral at a particular grade. It is defined as the surface area liberation (as determined using QEMSCAN) of the target mineral and is consequently directly related to the grind size utilised in the process. The results suggest that 65% grade of hematite can be theoretically recovered only at a recovery below 40% which means that it is impossible to remove the iron completely through physical beneficiation.

3.3 Magnetic separation

Magnetic separation studies were carried out in order to remove the locked iron particles understanding that the diaspore-rich fraction will report to the non-magnetic fraction. The bulk sample was ground to finer sizes such as 250, 125 and 75 μm for allowing complete liberation and then, subjected to WHIMS at three different magnetic intensities. The magnetic and non-magnetic products obtained were subjected to iron analysis and the details of the Fe grade and Fe recovery are listed in Table 5. The results clearly show that the non-magnetic fractions still contain more than 5% Fe irrespective of the grind size or magnetic intensity applied. The Fe recovery data show that a maximum of 48.9% of Fe is separable with WHIMS. These results further substantiate the fact that the iron-bearing phases are not liberated and more than 60% of the iron is still left in the diaspore-rich non-magnetic fraction even after applying the highest magnetic intensity at the lowest particle size. It may be noted that magnetic separation of samples below the sizes studied over here is not efficient and that is why was not considered.

The magnetic as well as non-magnetic products obtained from the magnetic separation (at 7700*G*) of the 75 μm sample were subjected to XRD analysis. The XRD pattern of the magnetic fraction as displayed in Fig. 10 confirms the presence of significant hematite peaks with less intense peaks of diaspore, kaolinite and chlorite whereas the XRD of the non-magnetic product suggested the enrichment of diaspore with less intense peaks of hematite, kaolinite, muscovite and apatite. The presence of hematite in the diaspore-rich non-magnetic fraction and diaspore in the magnetic fraction further suggests the problem of liberation of hematite validating the findings from the liberation and electron microscopic studies.

3.4 Leaching studies

Leaching studies in this work have been carried out using oxalic acid. Though, strong mineral acids such as HCl and H_2SO_4 are known to be good leachants of Fe, efforts have been made to establish an organic acid such as oxalic acid to leach out the iron present in diaspore. The sequence of chemical reactions between oxalic acid and iron oxide is as follows.

Oxalic acid ($H_2C_2O_4$), in aqueous solution, dissociates releasing the bi-oxalate ion, $HC_2O_4^-$ and protons H^+.

$$H_2C_2O_4 \rightarrow H^+ + HC_2O_4^- \quad (1)$$

The bi-oxalate ion further dissociates to oxalate ion, $C_2O_4^{2-}$:

$$HC_2O_4^- \rightarrow H^+ + C_2O_4^{2-} \quad (2)$$

Table 5 WHIMS of various size classified fractions along with iron analysis

Magnetic intensity, *G*	Product	250 μm			125 μm			75 μm		
		w/%	*w*(Fe)/%	Fe recovery/%	*w*/%	*w*(Fe)/%	Fe recovery/%	*w*/%	*w*(Fe)/%	Fe recovery/%
7700	Magnetic	7.25	35.99	33.03	12.31	28.50	44.41	9.68	31.27	38.32
	Non-magnetic	92.75	5.80		87.69	5.10		90.32	5.58	
11800	Magnetic	9.09	33.80	38.89	14.06	27.50	48.94	10.29	32.10	41.81
	Non-magnetic	90.91	5.34		85.94	5.01		89.71	5.45	
15400	Magnetic	9.84	33.08	41.20	13.43	27.50	46.75	11.43	31.50	45.58
	Non-magnetic	90.16	5.20		86.57	5.10		88.57	5.18	

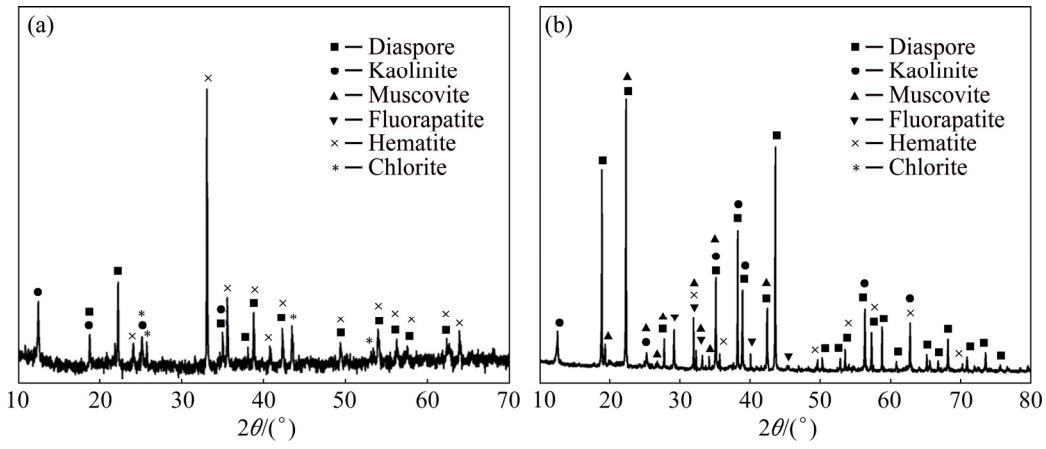

Fig. 10 XRD patterns of magnetic (a) and non-magnetic (b) fraction

The bi-oxalate ion causes the dissolution of the iron:

$$Fe_2O_3+H^++5HC_2O_4^-\rightarrow 2Fe(C_2O_4)_2^{2-}+3H_2O+2CO_2 \quad (3)$$

Thus, the dissolution of iron takes place by the formation of iron oxalate.

The dissolution behavior of the diaspore sample in oxalic acid was, initially, studied as a function of temperature and time. The sample having a size of below 38 μm was subjected to leaching in a 1 mol/L solution of oxalic acid while the temperature was varied from 45 to 90 °C and time from 15 to 120 min. The solid to liquid ratio was maintained at 1:10. The results as displayed in Fig. 11 show the leaching efficiency as a function of time and temperature. It is observed that the maximum leaching recorded at the temperatures 30, 45, 60, 75 and 90 °C to be 13.9%, 17.6%, 26.3%, 47.2% and 66.1%, respectively. The leaching efficiency is found to increase with an increase in temperature and time. For a time period of 120 min, the leaching efficiency increases from 13.9% to 66.1% as the temperature level is changed from 30 to 90 °C, suggesting that temperature has a great role to play in the dissolution of the iron present in the sample. However, it is to be noted that even with a leaching time of 120 min, a temperature of 90 °C and an acid concentration of 1 mol/L, the maximum leaching efficiency was found to be 66.1%. The EPMA based elemental mapping of the corresponding leached residue as displayed in Fig. 12 supports this result as fine locked grains of hematite can still be observed.

Further attempts were made to study the iron dissolution behavior with other factors of leaching such as acid concentration and solid to liquid ratio. The acid concentration was varied from 0.1 to 1 mol/L with the temperature and time fixed at 90 °C and 120 min respectively while the solid to liquid ratio was maintained at 0.1. In another set of experiments, the solid to liquid ratio was varied between 0.05 and 0.25 with a temperature of 90 °C, time of 120 min and acid concentration of 1 mol/L respectively. The results of

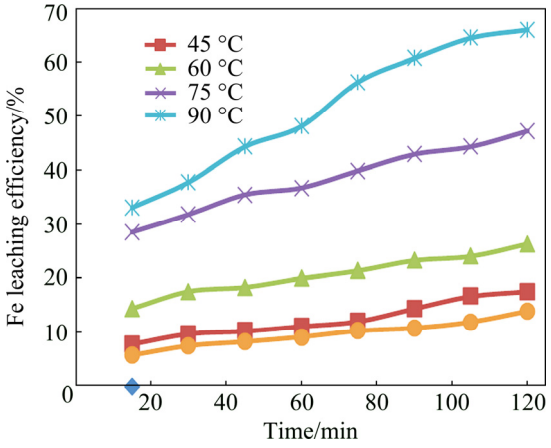

Fig. 11 Effect of leaching time and temperature on dissolution of iron from diaspore

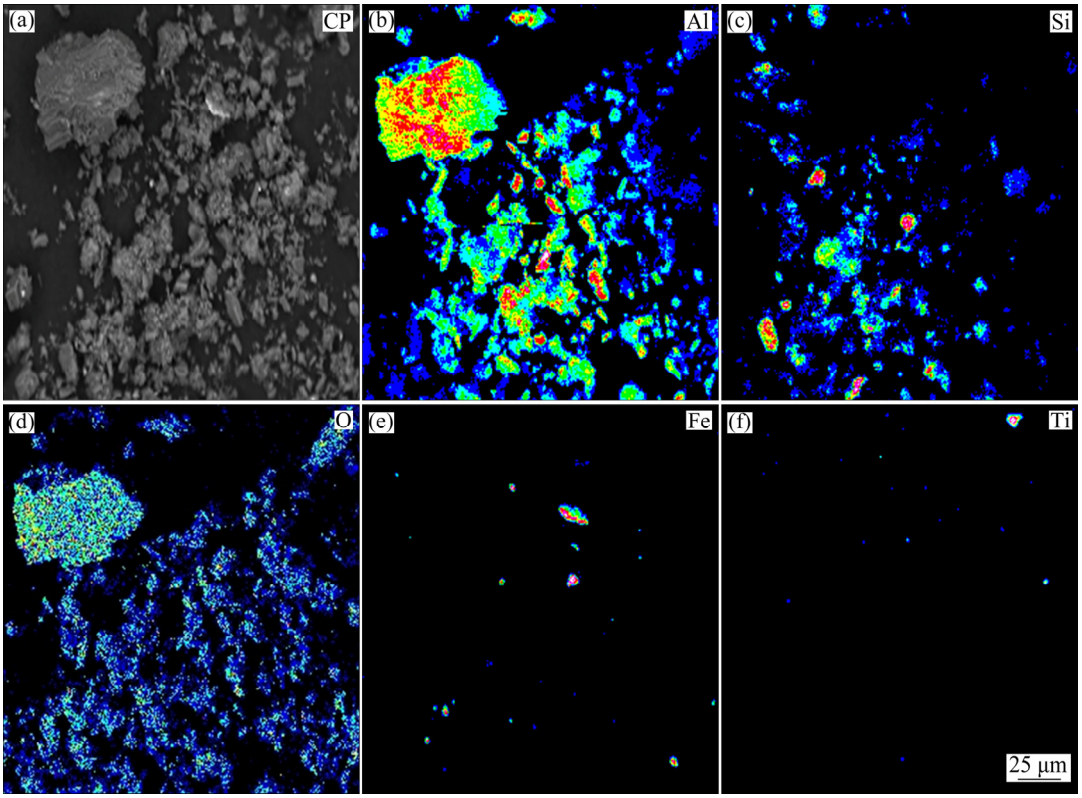

Fig. 12 Elemental distribution of Al, Si, O, Fe and Ti in leached residue of diaspore sample after being subjected to leaching at solid to liquid ratio of 0.1, temperature of 90 °C, time of 120 min and oxalic acid concentration of 1 mol/L

the studies involving the variation in acid concentration as displayed in Fig. 13(a) indicate that the decrease in acid concentration results in the decrease in Fe leaching. The leaching efficiency is as low as 13.4%, when the oxalic acid concentration is maintained at 0.1 mol/L. The effect of variation of solid to liquid ratio as plotted in Fig. 13(b) suggests that 76.3% of Fe is leachable at a solid to liquid ratio of 0.05:1. The leaching efficiency reduces to 35.2% as the ratio is increased to 0.25:1. However, considering the fact that a solid to liquid ratio of 0.05:1 is too low to be of industrial interest, the kinetics studies of the dissolution behavior were carried out with a solid to liquid ratio of 0.1:1.

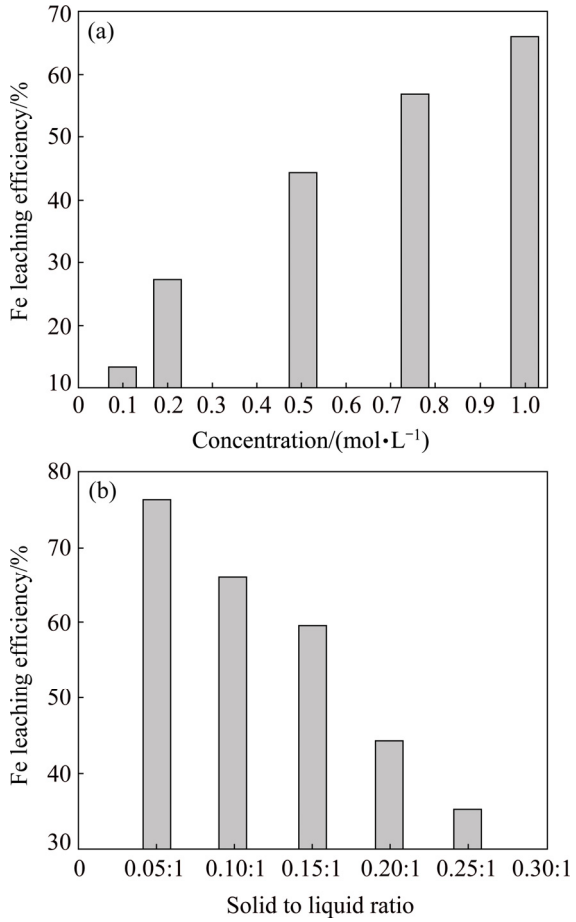

Fig. 13 Effect of acid concentration (a) and solid to liquid ratio (b) on dissolution of iron from diaspore

The complete analysis of the leached residue obtained at the optimal conditions such as solid to liquid ratio of 0.05:1, a temperature of 90 °C, an acid concentration of 1 mol/L and a contact time of 120 min was carried out. It was found to contain 2.14% Fe, 63.98% Al_2O_3, 17.5% SiO_2 and 15.03% LOI. Further, the analysis of the leached solution indicated that 2.13% of the Al_2O_3 present in the diaspore sample has leached into the oxalic acid solution.

There has been much attention on the studies of shrinking core models for the dissolution of metal ions from the ore body. As a reaction proceeds, the unreacted core size of the particle decreases gradually. For a heterogeneous system, the reaction rate is usually controlled by diffusion through the fluid film, diffusion through the ash or product layer and the chemical reaction on the surface of the particle or unreacted core [24,25]. Therefore, the following integrated rate equations were considered in order to study the reaction kinetics of iron dissolution from diaspore in the oxalic acid medium.

The integrated rate equations are given as

$$x=\frac{3bk_cC_A}{R\rho B}=k_ft \text{ (Film diffusion control)} \quad (4)$$

$$1-(1-x)^{1/3}=\left(\frac{k_cM_BC_A}{\rho_BbR}\right)t=k_rt$$

(Chemical reaction control) (5)

$$1-2(1-x)-3(1-x)^{2/3}=\left(\frac{2M_BDC_A}{\rho_BbR^2}\right)t=k_dt$$

(Ash diffusion) (6)

where x is the fraction leached, k_c is the kinetic constant, M_B is the relative molecular mass of the solid, C_A is the iron concentration in the solution, b is the stoichiometric coefficient, R is the initial radius of the solid particle, t is the reaction time, D is the diffusion coefficient in the porous product layer, ρ_B is the density of the solid particle, k_f, k_r and k_d are the rate constants.

The three different equations were investigated with respect to the linearization of the dissolution curves, and the corresponding rate constants and regression coefficients are shown in Table 6. The comparison of the values of the regression coefficients as obtained for different models suggests that there is hardly any difference among the values.

Further attempts were undertaken to determine the rate controlling mechanism using the activation energy data calculated using the initial rate method. Initial rate method has been regarded as one of the most efficient and unbiased method to study the kinetics [26]. In the present work, the leaching data were plotted against time for each temperature level and second order polynomial equations were fitted. The first derivatives of the polynomial equations calculated at time=0 were regarded as the initial rate. The initial rates (v_0) calculated at different temperatures were used to draw the Arrhenius plots of ln v_0 vs $1/T$ (Fig. 14). The apparent activation energy was calculated from the slope of the straight line (E/R, where E is the activation energy and R is the gas mole constant) as 35.15 kJ/mol. The estimated activation energy, which is less than 40 kJ/mol suggests that the leaching process is chemical reaction controlled [27,28].

Table 6 Linear regression coefficients for possible reaction mechanisms of leaching of iron from diaspore sample using oxalic acid at different temperatures

Model	30 °C		45 °C		60 °C		75 °C		90 °C	
	k	R^2	k	R^2	k	R^2	k	R^2	k	R^2
Film diffusion control	0.00070	0.979	0.00092	0.964	0.00105	0.984	0.00174	0.991	0.00354	0.974
Chemical reaction control	0.00025	0.978	0.00034	0.962	0.00041	0.985	0.00080	0.994	0.00190	0.986
Ash diffusion control	0.00005	0.946	0.00009	0.927	0.00017	0.984	0.00061	0.992	0.00188	0.988

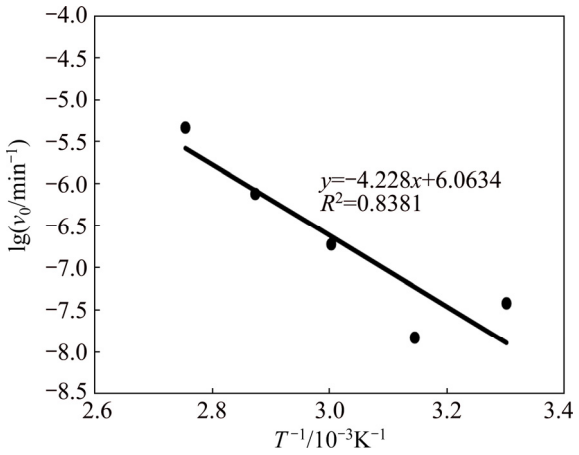

Fig. 14 Arrhenius plot for determination of activation energy

4 Conclusions

1) Phases like diaspore, kaolinite, fluorapatite and hematite were identified by XRD and further supplemented by SEM−EDS and EPMA studies, which also suggested a very complex association of the mineral phases present. The QEMSCAN based liberation studies further confirmed that only 40% of the hematite particles by mass have a degree of liberation of 90% or above even at the sizes below 38 μm.

2) Magnetic separation studies using WHIMS indicated that around 50% of the iron values were still left in the diaspore-rich non-magnetic fraction even at high magnetic intensities and fine particle sizes.

3) The leaching studies using oxalic acid could remove only 76.3% of the iron under optimum conditions such as solid to liquid ratio 0.05:1, temperature 90 °C, time 120 min and acid concentration 1 mol/L. The residue was found to contain 2.14% Fe. It was also observed that with a solid to liquid ratio of 0.1:1, the leaching efficiency was limited to 66.1%. The results clearly suggest that the liberation problem associated with the iron phases are also a hindrance in the process of leaching, and more leaching time and less solid to liquid ratio may lead to a better leaching efficiency.

4) Overall, the present study puts forward a picture of the liberation issues in diaspore responsible for difficulties in the removal of iron and provides the preliminary data of iron dissolution kinetics in oxalic acid.

Acknowledgments

The authors are thankful to the Director, CSIR-IMMT, Bhubaneswar for his kind permission to publish this paper.

References

[1] CHESTER R, JONES F, LOAN M, OLIVEIRA A, RICHMOND W. The dissolution behaviour of titanium oxide phases in synthetic Bayer liquors at 90 °C [J]. Hydrometallurgy, 2009, 96: 215−222.

[2] Indian Minerals Yearbook, Part III: Mineral Reviews [M]. 53rd Edition, 2014.

[3] REDDY B R, MISHRA S K, BANERJEE G N. Kinetics of leaching of a gibbsitic bauxite with hydrochloric acid [J]. Hydrometallurgy, 1999, 51: 131−138.

[4] LEE S O, TRAN T, PARK Y Y, KIM S J, KIM M J. Study on the kinetics of iron oxide leaching by oxalic acid [J]. International Journal of Mineral Processing, 2006, 80: 144−152.

[5] BHAGAT R P, BANERJEE B, KUNWAR R K, DEY S. Beneficiation tests on an Indian bauxite incorporating magnetic separation [J]. Transactions of the Institute of Mining and Metallurgy, Section C, 2001, 110: C165−C168.

[6] MACIEJEWSKI M, RICHARZ W. Reduction of iron oxides in bauxite by hydrogen [J]. Thermochimica Acta, 1985, 85: 199−202.

[7] SADLE L Y, VENKATARAMAN C. A process for enhanced removal of iron from bauxite ores [J]. International Journal of Mineral Processing, 1991, 31(3−4): 233−246.

[8] PAPASSIOPI N, VAXEVANIDOU K, PASPALIARIS I. Effectiveness of iron reducing bacteria for the removal of iron from bauxite ores [J]. Minerals Engineering, 2010, 23(1): 25−31.

[9] SALEHI S, NOAPARAST M, SHAFAEI S Z, AMINI A, HEIDARNIA A. Iron leaching from bauxite ore in hydrochloric acid using response surface methodology [J]. Journal of Mining and Environment, 2015, 6(1): 103−108.

[10] PASPALIARIS Y, TSOLAKIS Y. Reaction kinetics for the leaching of iron oxides in diasporic bauxite from the Parnassus-Giona Zone (Greece) by hydrochloric acid [J]. Hydrometallurgy, 1987, 19: 259−266.

[11] GÜLFEN G, GÜLFEN M, AYDIN A O. Dissolution kinetics of iron from diaspore bauxite in hydrochloric acid solution [J]. Indian Journal of Chemical Technology, 2006, 13: 386−390.

[12] LI Guang-hui, GU Fo-quan, JIANG Tao, LUO Jun, DENG Bo-na, PENG Zhi-wei. Beneficiation of Aluminum-, Iron-, and titanium-bearing constituents from diasporic bauxite ores [J]. JOM: The Journal of the Minerals, Metals & Materials Society (TMS), 2017, 69(2): 315−322.

[13] JIANG T, YANG L, LI G, LUO J, ZENG J, PENG Z, LIU M. (2016) Separation of aluminium and preparation of powdered DRI from

lateritic iron ore based on direct reduction process [J]. Canadian Metallurgical Quarterly, 2016, 55: 345−355.
[14] LI Guang-hui, JIANG Tao, LIU Mu-dan, ZHOU Tai-hua, FAN Xiao-hui, QIU Gaun-zhou. Beneficiation of high-aluminium-content hematite ore by soda ash roasting [J]. Mineral Processing and Extractive Metallurgy Review, 2010, 31: 150−164.
[15] LI Guang-hui, LIU Ming-xia, RAO Ming-jun, JIANG Tao, ZHUANG Jin-qiang, ZHANG Yuan-bo. Stepwise extraction of valuable components from red mud based on reductive roasting with sodium salts [J]. Journal of Hazardous Materials, 2014, 280: 774−780.
[16] HU Yue-hua. Progress in flotation de-silica [J]. Transactions of Nonferrous Metals Society of China, 2003, 13(3): 656−662.
[17] XIA Liu-yin, ZHONG Hong, LIU Guang-yi. Flotation techniques for separation of diaspore from bauxite using Gemini collector and starch depressant [J]. Transactions of Nonferrous Metals Society of China, 2010, 20 (3): 495−501.
[18] JIANG Hao, XU Long-hua, HU Yue-hua, WANG Dian-zuo, WANG Xing-jie. Flotation and adsorption of quaternary ammonium cationic collectors on diaspore and kaolinite [J]. Transactions of Nonferrous Metals Society of China, 2011, 21(11): 2528−2534.
[19] LI Hai-pu, ZHANG Sha-sha, JIANG Hao, LI Bin, LI Xing. Effect of degree of substitution of carboxymethyl starch on diaspore depression in reverse flotation [J]. Transactions of Nonferrous Metals Society of China, 2011, 21(8): 1868−1873.
[20] LI Hai-pu, ZHANG Sha-sha, JIANG Hao, LI Bin. Effect of modified starches on depression of diaspore [J]. Transactions of Nonferrous Metals Society of China, 2010, 20 (8): 1494−1499.
[21] MOLLAI H. Role of mineralogy and geochemistry in the beneficiation of Jajarm bauxite from north east Iran: Comparison with some other bauxite deposits of the world [J]. Iranian Journal of Earth Sciences, 2011, 3: 153−167.
[22] RAO D S, DAS B. Characterization and beneficiation studies of a low grade bauxite ore [J]. Journal of the Institution of Engineers (India): Series D, 2014, 95(2): 81−93.
[23] PANDA S, MISHRA S, RAO D S, PRADHAN N, MOHAPATRA U, ANGADI S, MISHRA B K. Extraction of copper from copper slag: Mineralogical insights, physical beneficiation and bioleaching studies [J]. Korean Journal of Chemical Engineering, 2015, 32(4): 667−676.
[24] DENG C H, FENG Q M, CHEN Y. Studies on the leaching kinetics of cobalt from spent catalyst with sulphuric acid [J]. Mineral Processing & Extractive Metallurgy, 2007, 116(3): 159−162.
[25] LEVENSPIEL O. Chemical reaction engineering [M]. New York: John Wiley and Sons, 1972: 566−586.
[26] CASADO J, LOPEZ-QUINTELA M A, LORENZO-BARRAL F M. The initial rate method in chemical kinetics: Evaluation and experimental illustration [J]. Journal of Chemical Education, 1986, 63(5): 450−452.
[27] SOUZA A D, PINA P S, LEAO V A, SILVA C A, SIQUEIRA P F. The leaching kinetics of a zinc sulphide concentrate in acid ferric sulphate [J]. Hydrometallurgy, 2007, 89: 72−81.
[28] ADEBAYO A O, IPINMOROTI K O, AJAYI O O. Leaching of sphalerite with hydrogen peroxide and nitric acid solutions [J]. Journal of Minerals & Materials Characterization & Engineering, 2006, 5(2): 167−177.

印度一水硬铝石样品中氧化铁相的矿物学、解离和浸出特性

Danda Srinivas RAO, Swagat S. RATH, Nilima DASH, Swagatika MOHANTY, Surendra K. BISWAL

Council of Scientific and Industrial Research, Institute of Minerals and Materials Technology, Bhubaneswar 751013, India

摘　要：利用磁选和浸出技术从印度一水硬铝石样品中除铁，采用扫描电镜、电子探针显微分析仪和 X 射线衍射等定量矿物学评价技术进行深入的矿物学表征研究。结果表明，极细的赤铁矿颗粒与其他几种矿物相以复杂的方式结合在一起；即使粒度小于 38 μm，仍有约 60%的赤铁矿未被解离出来；这个粒度也是物理分离过程去铁的极限。湿式强磁选研究表明，只有 49%的铁可被除去。进一步的草酸浸出研究表明，在固液比 0.05:1、温度 90 °C、时间 120 min、酸浓度 1 mol/L 的条件下，可除去约 76%的铁。铁在草酸中的溶解受化学反应控制，计算的活化能为 35.15 kJ/mol。

关键词：一水硬铝石；解离；矿物学；浸出；磁选

(Edited by Xiang-qun LI)